

# Modeling and Analysis of Multi-frequency Mechanical Forced Oscillations in Power Systems

Erick Davalos

*Graduate Program in Electrical Engineering  
University of Guadalajara  
Guadalajara, Jalisco, Mexico  
erick.davalos2937@alumnos.udg.mx*

Emilio Barocio

*Electrical Engineering Department  
University of Guadalajara  
Guadalajara, Jalisco, Mexico  
emilio.barocio@academicos.udg.mx*

**Abstract**—Forced oscillations (FO) in power systems can produce large sustained responses, distort measurements and threaten system stability. Although often modeled as single sinusoidal inputs, many practical sources generate non-sinusoidal periodic disturbances composed of multiple harmonics. This paper analyzes a single machine infinite bus (SMIB) system subjected to multi-frequency mechanical forcing modeled by a finite Fourier series. Closed-form expressions are derived using a Laplace domain formulation that separates modal dynamics from the forced response of each harmonic. Results illustrate how operating conditions and spectral composition shape the oscillatory response and sensitivity to forcing.

**Index Terms**—Multi-frequency forced oscillations, power systems, resonance, frequency-domain analysis, Fourier series.

## I. INTRODUCTION

Forced oscillations have emerged as a significant and recurring phenomenon in power systems, characterized by sustained periodic responses driven by persistent disturbances rather than by intrinsic modal dynamics [1]. Unlike natural oscillations, which decay due to system damping, forced oscillations persist while the external disturbance remains active and can reach amplitudes substantially larger than the forcing, posing a significant threat to power system stability [2].

A broad range of mechanisms can generate forced oscillations, including cyclic loads, turbine–governor interactions, malfunctioning of control loops/mechanical devices and converter-based generation [3] [4]. When injected into a power system, these disturbances can propagate geographically and interact with natural modes, causing measurement distortions that may trigger false alarms [5]. Moreover, such interactions may degrade stability margins, reduce power transfer capability and in severe cases lead to blackouts [6]. With the widespread deployment of phasor measurement units (PMUs), forced oscillations have become more visible in power networks, motivating efforts to understand their mechanisms. As a result, developing accurate models and analytical methods to explain, predict and quantify these phenomena is crucial for dynamic security assessment and system monitoring.

Most analytical studies represent these disturbances as single sinusoidal inputs, which simplifies analysis and aligns

This work was supported by the national agency SECIHTI in Mexico under grant CVU: 2056858.

with conventional spectral interpretation [7] [8]. While this approach has delivered valuable insight into resonance and detection concepts, it struggles to reflect the spectral richness of realistic disturbances. In practice, many periodic mechanisms produce waveforms that are non-sinusoidal but periodic [5] [9], meaning that the disturbance contains multiple harmonics that might interact with natural modes. Some studies have examined square wave inputs, showing that the output is a sum of harmonic components shaped by system dynamics [10].

The previous studies highlight the need for a detailed analysis that treat the disturbance not as a single tone, but as a general periodic input. This work seeks to characterize forced oscillations under a disturbance representation that explicitly preserves their multi-frequency nature.

To this end, the disturbance is modeled as a finite Fourier series, offering a mathematically compact and meaningful way to describe periodic inputs. The analysis considers a classical synchronous generator under a multi-frequency mechanical periodic perturbation connected to an infinite bus as shown in Fig. 1. Because the swing equation is linearized around an operating point, the response to each harmonic can be obtained independently and superimposed through the principle of linearity. This simple yet representative model allows closed-form analysis and clear visualization of interference effects.

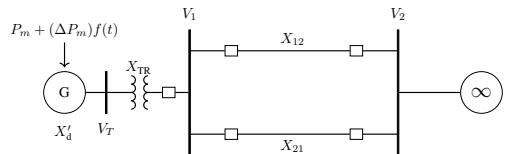


Fig. 1. A single synchronous machine with mechanical forcing  $\Delta P_m$  connected to an infinite bus system.

Section II presents the SMIB system under Fourier series forcing and derives analytical expressions for its response using a Laplace domain formulation, which captures both transient and steady-state behavior and naturally accommodates the superposition of multiple harmonics through algebraic manipulation of system poles. Section III analyzes these results through examples illustrating how system parameters affect sensitivity to forced oscillations and how the spectral composition of the input shapes the system dynamics.

## II. MATHEMATICAL FORMULATION AND ANALYTICAL SOLUTION OF THE SYSTEM

### A. System Model

Given the linearized forced swing equation in (1), the Laplace transform is applied to obtain expressions that explicitly separates the natural (modal) response from the input dynamics.

$$\frac{d^2\Delta\delta}{dt^2}dELTA + 2\zeta\omega_n \frac{d\Delta\delta}{dt} + \omega_n^2\Delta\delta = \underbrace{\gamma \left[ \frac{a_0}{2} + \sum_{k=1}^N (a_k \cos(k\omega t) + b_k \sin(k\omega t)) \right]}_{F_S(t)} \quad (1)$$

Where the Fourier coefficients  $(a_0, a_k, b_k)$  and the system parameters  $(\omega_n, \zeta, \gamma)$  are presented in equation (2).  $N$  is the number of harmonics considered in the series.

$$\begin{aligned} \omega_n^2 &= \frac{P_{max} \cos(\delta_0 - \theta) \omega_s}{2H}, \quad \zeta\omega_n = \frac{D\omega_s}{4H}, \\ \gamma &= \Delta P_m \frac{\omega_s}{2H}, \quad a_k = \frac{2}{T} \int_0^T f(t) \cos(k\omega t) dt \\ a_0 &= \frac{2}{T} \int_0^T f(t) dt, \quad b_k = \frac{2}{T} \int_0^T f(t) \sin(k\omega t) dt \end{aligned} \quad (2)$$

The disturbance magnitude is denoted by  $\Delta P_m$ ,  $\omega_s$  is the synchronous speed and the maximum power transfer  $P_{max}$  is given by  $V_i V_j / X_{ij}$ , where  $V_i$  and  $V_j$  are the bus voltages across the reactance  $X_{ij}$ . The mechanical perturbation is modeled as  $\Delta P_m f(t)$ , where  $f(t)$  is a periodic waveform of period  $T$  represented by its Fourier series, with harmonics indexed by  $k$ . In the swing equation in (1), this disturbance appears as the forcing term  $F_S(t) = \gamma f(t)$ . The expression for  $\omega_n$  in (2) shows that operation near the stability limit  $(\delta_0 - \theta) \rightarrow \pi/2$  reduces the synchronizing coefficient  $K_S = P_{max} \cos(\delta_0 - \theta)$  which results in slower oscillations and weaker restoring torque. Increasing  $K_S$  makes the system stiffer and increases  $\omega_n$ , shifting the modes to a higher frequency, producing a more oscillatory transient, even though the decay rate is constant for fixed  $D$  and  $H$  since the real part of natural modes is  $-\zeta\omega_n$ .

### B. Modal Decomposition Through the Laplace Transform

Applying the Laplace transform to equation (1) and using initial conditions  $\Delta\delta(0) = \Delta\delta_0$  and  $\Delta\dot{\delta}(0) = \Delta\omega_0$  gives:

$$[s^2\Delta\delta(s) - s\Delta\delta_0 - \Delta\omega_0] + 2\zeta\omega_n[s\Delta\delta(s) - \Delta\delta_0] + \omega_n^2\Delta\delta(s) = F_S(s) \quad (3)$$

Solving for the angle displacement  $\Delta\delta(s)$  and separating the overall solution in its purely intrinsic response depending only on initial conditions and the forced dynamics regarding the Fourier series power disturbance  $F_S(s)$ , it yields:

$$\Delta\delta(s) = \underbrace{\frac{\Delta\delta_0(2\zeta\omega_n + s) + \Delta\omega_0}{(s - r_1)(s - r_2)}}_{\text{Zero Input Response (ZIR)}} + \underbrace{\frac{F_S(s)}{(s - r_1)(s - r_2)}}_{\text{Zero State Response (ZSR)}}, \quad (4)$$

$$r_{1,2} = -\zeta\omega_n \pm j \underbrace{\omega_n \sqrt{1 - \zeta^2}}_{\omega_d}$$

Note that both denominators are the same, this means that the system poles (eigenvalues) are excited through initial conditions  $[\Delta\delta_0, \Delta\omega_0]$  or merely by the forcing  $F_S(s)$ . This decomposition cleanly separates the transient modal dynamics from the forced input contribution.

To obtain the time domain solution, we must expand each term of equation (4) using partial fraction decomposition to obtain the scaling residues for each mode and then apply the inverse Laplace transform.

### C. Zero Input Response (ZIR)

Recalling the term corresponding to the ZIR in equation (4) and expanding using partial fractions yields:

$$\Delta\delta_{ZI}(s) = \frac{s\Delta\delta_0 + 2\zeta\Delta\delta_0\omega_n + \Delta\omega_0}{(s - r_1)(s - r_2)} = \frac{A}{s - r_1} + \frac{B}{s - r_2} \quad (5)$$

Because the system coefficients are real, the characteristic roots  $r_1$  and  $r_2$  form a complex conjugate pair which forces the residues to also be complex conjugates. This let us to solve for  $A$  and define  $B$  simply as the conjugate of  $A$ . This turns to be  $B = A^*$  where the upper asterisk represents the conjugate.

$$A = \frac{\Delta\delta_0}{2} - \frac{j}{2\sqrt{1 - \zeta^2}} \left( \frac{\Delta\omega_0}{\omega_n} + \zeta\Delta\delta_0 \right) \quad (6)$$

Applying the inverse Laplace transform to obtain  $\Delta\delta_{ZI}(t)$ :

$$\Delta\delta_{ZI}(t) = 2\Re\{Ae^{(-\zeta\omega_n + j\omega_d)t}\} \quad (7)$$

### D. Zero State Response (ZSR)

The second term of equation (4) associated to the ZSR can be rewritten explicitly as follows:

$$\begin{aligned} \Delta\delta_{ZS}(s) &= \frac{\gamma}{(s - r_1)(s - r_2)} \left[ \frac{a_0}{2} \left( \frac{1}{s} \right) + \dots \right. \\ &\quad \left. + \sum_{k=1}^N \left( a_k \frac{s}{s^2 + (k\omega)^2} + b_k \frac{k\omega}{s^2 + (k\omega)^2} \right) \right] \end{aligned} \quad (8)$$

The system poles also affect each forcing term, one related to the constant or DC component and two associated with the cosine and sine terms respectively. By linearity the solution can be obtain by adding each solution separately.

$$\Delta\delta_{ZS}(s) = U_{DC}(s) + U^{(cos)}(s) + U^{(sin)}(s) \quad (9)$$

Using partial fraction decomposition to obtain  $U_{DC}(s)$  which is the contribution of the DC term to the ZSR:

$$U_{DC}(s) = \frac{\gamma a_0}{2} \left[ \frac{A_0}{s} + \frac{B_0}{s - r_1} + \frac{C_0}{s - r_2} \right] \quad (10)$$

The residues  $A_0, B_0$  and  $C_0$  are:

$$\begin{aligned} A_0 &= \frac{1}{\omega_n^2}, \\ B_0 &= \frac{1}{2\omega_n^2} \left[ -1 + j \frac{\zeta}{\sqrt{1 - \zeta^2}} \right], \quad C_0 = B_0^* \end{aligned} \quad (11)$$

Hence, the time solution of the DC term is:

$$U_{DC}(t) = \frac{\gamma a_0}{2} \left[ A_0 + B_0 e^{r_1 t} + C_0 e^{r_2 t} \right] \quad (12)$$

The next term to be analyzed corresponds to the  $U^{(cos)}(s)$  term, which has a cosine function and only even harmonics.

$$U^{(cos)}(s) = \gamma \left\{ \sum_{k=1}^N \left[ a_k \left( \frac{A_{k,r_1}}{s - r_1} + \frac{A_{k,r_2}}{s - r_2} \right) + \dots + \frac{B_{k,1}}{s + jk\omega} + \frac{B_{k,2}}{s - jk\omega} \right] \right\} \quad (13)$$

Residues  $A_{k,r_1}$  and  $A_{k,r_2}$  correspond to the transient contribution of the forcing cosine via the natural poles. While  $B_{k,1}$  and  $B_{k,2}$  are associated to the steady state forced solution.

$$\begin{aligned} A_{k,r_1} &= \frac{1}{2\omega_n^2} \left[ \frac{(\Omega^2 - 1) + j\frac{\zeta}{\sqrt{1-\zeta^2}}(\Omega^2 + 1)}{(1 - \Omega^2)^2 + (2\zeta\Omega)^2} \right], \\ B_{k,1} &= \frac{1}{2\omega_n^2} \left[ \frac{(1 - \Omega^2) + j(2\zeta\Omega)}{(1 - \Omega^2)^2 + (2\zeta\Omega)^2} \right], \end{aligned} \quad (14)$$

$$A_{k,r_2} = A_{k,r_1}^*, \quad B_{k,2} = B_{k,1}^*$$

Where  $\Omega$  is defined as the ratio between the harmonic frequency and the natural frequency of the system ( $\Omega = k\omega/\omega_n$ ). The contribution in time of the Fourier series cosine terms to the ZSR is:

$$\begin{aligned} U^{(cos)}(t) &= \gamma \sum_{k=1}^N a_k \left( A_{k,r_1} e^{r_1 t} + A_{k,r_2} e^{r_2 t} + \dots + B_{k,1} e^{-jk\omega t} + B_{k,2} e^{+jk\omega t} \right) \end{aligned} \quad (15)$$

Now, to get the sine contribution  $U^{(sin)}(s)$  to the ZSR, same procedure as before is conducted.

$$\begin{aligned} U^{(sin)}(s) &= \gamma \left\{ \sum_{k=1}^N \left[ b_k \left( \frac{C_{k,r_1}}{s - r_1} + \frac{C_{k,r_2}}{s - r_2} \right) + \dots + \frac{D_{k,1}}{s + jk\omega} + \frac{D_{k,2}}{s - jk\omega} \right] \right\} \end{aligned} \quad (16)$$

Residues  $C_{k,r_1}$  and  $C_{k,r_2}$  similarly correspond to the transient contribution of the forcing sine via the natural poles. While  $D_{k,1}$  and  $D_{k,2}$  affect the steady state response.

$$\begin{aligned} C_{k,r_1} &= \frac{\Omega}{2\omega_n^2} \left[ \frac{2\zeta - j\frac{\Omega^2 + 2\zeta^2 - 1}{\sqrt{1-\zeta^2}}}{(1 - \Omega^2)^2 + (2\zeta\Omega)^2} \right], \\ D_{k,1} &= -\frac{1}{2\omega_n^2} \left[ \frac{(2\zeta\Omega) - j(1 - \Omega^2)}{(1 - \Omega^2)^2 + (2\zeta\Omega)^2} \right], \end{aligned} \quad (17)$$

$$C_{k,r_2} = C_{k,r_1}^*, \quad D_{k,2} = D_{k,1}^*$$

The time domain contribution of the Fourier series sine terms to the ZSR is:

$$\begin{aligned} U^{(sin)}(t) &= \gamma \sum_{k=1}^N b_k \left( C_{k,r_1} e^{r_1 t} + C_{k,r_2} e^{r_2 t} + \dots + D_{k,1} e^{-jk\omega t} + D_{k,2} e^{+jk\omega t} \right) \end{aligned} \quad (18)$$

#### E. Power Angle Total Solution

To construct the time domain solution lets look into the equations (7), (12), (15) and (18). These four equations add up into the power angle solution, it is known that  $\Delta\delta(t) = \Delta\delta_{ZI}(t) + \Delta\delta_{ZS}(t)$ . Thus, factorizing each term with its corresponding oscillatory mode and considering that the residues come in complex conjugates with real coefficients  $a_k, b_k$  we get the equation (19).

$$\begin{aligned} \Delta\delta(t) &= \frac{\gamma a_0}{2} A_0 + 2 \Re \left\{ e^{-\zeta\omega_n t} \left[ \underbrace{A + \frac{\gamma a_0}{2} B_0}_{C_{r_1}^{\text{TOT}}} + \right. \right. \\ &\quad \left. \left. + \underbrace{\gamma \sum_{k=1}^N (a_k A_{k,r_1} + b_k C_{k,r_1})}_{C_{r_1}^{\text{TOT}}} \right] e^{j\omega_d t} \right. \\ &\quad \left. + \gamma \sum_{k=1}^N \underbrace{(a_k B_{k,2} + b_k D_{k,2})}_{C_k^{\text{SS}}} e^{jk\omega t} \right\} \end{aligned} \quad (19)$$

#### F. Power Angle Total Solution Envelope

The envelope is given by the modulus of the analytic signal  $a_{\Delta\delta}(t) = |\Delta\delta(t)| = [\Delta\hat{\delta}(t)\Delta\hat{\delta}^*(t)]^{1/2}$ . To construct the analytic signal of the equation (19), transient ( $C_{r_1}^{\text{TOT}}$ ) and steady-state ( $C_k^{\text{SS}}$ ) contributions are grouped into their corresponding complex coefficients.

$$\Delta\hat{\delta}(t) = \underbrace{2C_{r_1}^{\text{TOT}} e^{-(\zeta\omega_n - j\omega_d)t}}_{Z_T^{\text{TOT}}(t)} + \underbrace{\left( \frac{\gamma a_0}{2} A_0 + 2\gamma \sum_{k=1}^N C_k^{\text{SS}} e^{jk\omega t} \right)}_{Z_F^{\text{SS}}(t)} \quad (20)$$

To obtain a representative closed envelope expression the identity  $|Z_T^{\text{TOT}}(t) + Z_F^{\text{SS}}(t)|^2$  is used. This gives the power angle envelope expression shown in equation (21).

$$\begin{aligned} a_{\Delta\delta}(t) &= \left[ |Z_T^{\text{TOT}}(t)|^2 + |Z_F^{\text{SS}}(t)|^2 \right. \\ &\quad \left. + 2 \Re \left\{ Z_T^{\text{TOT}}(t) Z_F^{\text{SS}*}(t) \right\} \right]^{1/2} \end{aligned} \quad (21)$$

For clarity, each term in (21) is expanded explicitly using definitions stated in equation (20), resulting in equation (22).

$$\begin{aligned}
a_{\Delta\delta}(t) = & \left[ \underbrace{\left| 2C_{r_1}^{\text{TOT}} \right|^2 e^{-2\zeta\omega_n t}}_{\text{decaying term}} + \underbrace{\left| \frac{\gamma a_0}{2} A_0 \right|^2 + 4\gamma^2 \sum_{k=1}^N |C_k^{\text{SS}}|^2}_{\text{constant terms}} \right. \\
& + \underbrace{4\gamma \Re \left\{ \left( \frac{\gamma a_0}{2} A_0 \right) \sum_{k=1}^N C_k^{\text{SS}*} e^{-jk\omega t} \right\}}_{\text{forcing frequencies } k\omega} \\
& + \underbrace{8\gamma^2 \Re \left\{ \sum_{k=1}^N \sum_{\ell>k} C_k^{\text{SS}} C_\ell^{\text{SS}*} e^{j(k-\ell)\omega t} \right\}}_{\text{forcing difference frequencies } (k-\ell)\omega} \\
& + \underbrace{2e^{-\zeta\omega_n t} \Re \left\{ 2C_{r_1}^{\text{TOT}} \left( \frac{\gamma a_0}{2} A_0 \right)^* e^{j\omega_d t} \right\}}_{\text{decaying oscillation at } \omega_d} \\
& \left. + 2e^{-\zeta\omega_n t} \sum_{k=1}^N \Re \left\{ 4\gamma C_{r_1}^{\text{TOT}} C_k^{\text{SS}*} e^{j(\omega_d-k\omega)t} \right\} \right]^{1/2} \\
& \quad \underbrace{\text{decaying beat frequencies } (\omega_d-k\omega)}_{(22)}
\end{aligned}$$

Equation (22) shows that the envelope is a nonlinear (modulus) function of transient and steady-state terms. The factor  $e^{-2\zeta\omega_n t}$  originates from  $|Z_T^{\text{TOT}}(t)|^2$  and reflects the exponential decay of the natural mode governed by the damping ratio. The sum  $4\gamma^2 \sum |C_k^{\text{SS}}|^2$  quantifies the steady-state contribution of the forcing harmonics. The double sum over  $k$  and  $\ell$  arises because each harmonic multiplies every other harmonic when forming  $|Z_F^{\text{SS}}(t)|^2$ ; these cross-terms oscillate at the difference frequencies  $(k-\ell)\omega$  and produce modulation in the envelope. Finally, the terms  $e^{-\zeta\omega_n t} e^{j(\omega_d-k\omega)t}$  represent damped interactions between the transient mode and each forcing harmonic, generating beat frequencies at  $(\omega_d - k\omega)$ .

### III. SIMULATION AND ANALYSIS

The parameters of the test system in Fig. 1 are expressed in per unit on the same base as the machine power rating. A 100 MVA hydro power synchronous generator with an inertia constant  $H = 3.55$  supplying 60MW at 0.9 lagging power factor is considered, its transient reactance is  $X'_d = 0.3$ , transformer reactance  $X_{\text{TR}} = 0.1$ , line reactances  $X_{12} = 0.2$  and  $X_{21} = 0.3$ , terminal voltage setpoint  $V_T = 1.05$ , infinite bus voltage  $V_2 = 1.0$  and synchronous speed  $\omega_s = 377$  rad/s.

The two transmission lines in parallel give  $X_{||} = 0.12$ , so the equivalent transfer reactance between the internal voltage  $E'$  and  $V_2$  is  $X_{\text{eq}} = 0.52$ . Using the classical model, the magnitude of the internal voltage is  $|E'| = 1.15$  p.u. Hence the maximum electrical power is  $P_{\text{max}} = 2.20$  p.u and the corresponding steady state angle is  $\delta_0 = 0.276$  rad =  $15.8^\circ$ . The actual electrical power is  $P_e = P_{\text{max}} \sin(\delta - \theta)$  where  $\theta = 0$  is the infinite bus angle.

### A. Influence of Parameters on Forced Oscillations

The natural frequency of the linearized SMIB depends on the synchronizing coefficient  $K_s = P_{\text{max}} \cos(\delta_0)$  and on the inertia  $H$ , as defined in equation (2). Stronger electrical coupling increases  $P_{\text{max}}$  and raises  $\omega_n$ , whereas operating near the stability limit reduces the synchronizing torque and slows the oscillations. Larger inertia decreases  $\omega_n$ , making the system respond more slowly and shifting the resonance region. These trends are shown in Fig. 2 and were plotted using (2).

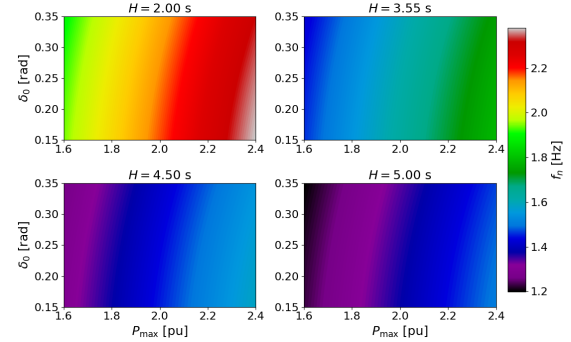


Fig. 2. SMIB natural frequency variation with operating point and inertia.

In the frequency domain, parameter changes manifest as different resonance shapes as shown in Fig. 3. Case (a): a larger disturbance magnitude  $\Delta P_m$  scales the forcing term  $\gamma$  in (1) and increases the magnitude of the harmonic components in (15) and (18), the strongest effect is at resonance. Case (b): damping  $D$  has a dominant influence: higher values reduce the resonant peak while leaving the off-resonant response almost unchanged. Case (c): inertia has a secondary but noticeable effect; when other parameters are fixed, larger  $H$  produces slightly higher gains because  $\omega_n$  decreases with  $H$  and the residues scale with  $1/\omega_n^2$  according to (14) and (17). This amplification is weaker than the effect of  $\Delta P_m$  or  $D$ .

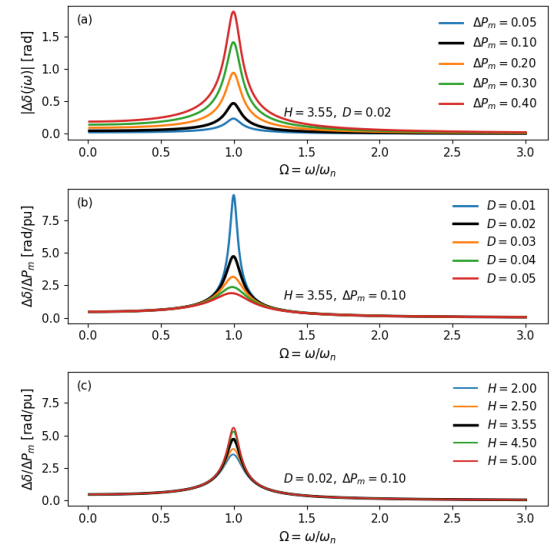


Fig. 3. Steady-state frequency response obtained from equation (4) for different values of  $\Delta P_m$ ,  $D$ , and  $H$ .

Fig. 4 presents a three-dimensional plot of the power angle envelope calculated in equation (22) as a function of time and  $\Omega$ , with color indicating the incremental kinetic energy of the rotor. The energy was computed according to equation (23).

$$E_\Delta = HS_{\text{base}} \left( \frac{\Delta\dot{\delta}}{\omega_s} \right)^2 \quad (23)$$

It quantifies the kinetic energy stored in the rotor relative to the synchronous operating point, it is directly proportional to the square of the relative speed deviation [ $\dot{\delta} = \Delta\omega(t)$ ]. The strongest activity is observed near  $\Omega = 1$ , reflecting resonance amplification when the forcing frequency aligns with the natural frequency of the system, resulting in maximum energy transfer into the rotor dynamics.

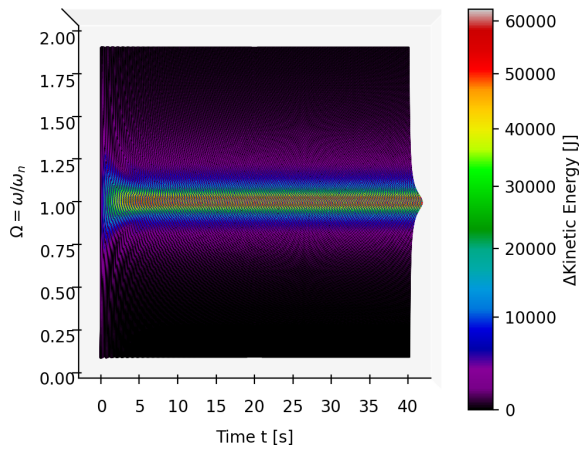


Fig. 4. Synchronous generator power angle envelope colored by incremental kinetic energy over time during a frequency sweep.

## B. Single-Tone and Harmonic Forced Resonance Analysis

Considering the parameters defined at the beginning of this section, the resulting natural frequency is  $\omega_n = 10.6$  rad/s (1.69 Hz) and the damping ratio is  $\zeta = 5\%$  when the overall damping is taken as  $D = 0.02$ . The input gain given a mechanical disturbance amplitude  $\Delta P_m = 0.1$  is  $\gamma = 5.31$  and the number of harmonics chosen is  $N = 15$ . An input with fundamental frequency of one fifth of the natural frequency is chosen,  $\omega = \omega_n/5 \approx 0.34$  Hz, no DC component is considered since it only shifts the operating point. The initial condition for the following is set to  $\Delta\delta_0 = 0.2$  rad.

Figure 5 shows the SMIB response under different periodic forcings. The time domain waveforms obtained from nonlinear numerical integration (first column) closely match the analytical solution in (19), confirming that the modal decomposition in (4) accurately captures the dominant electromechanical dynamics despite the linear approximation. Single-tone excitation yields a large sinusoidal response when the forcing frequency is near  $\omega_n$ , whereas multi-harmonic inputs excite resonances whenever  $k\omega_f \approx \omega_n$ , producing irregular trajectories due to the superposition of several near resonance components with different phases and amplitudes.

The FFT of  $\Delta\delta(t)$  (second column) highlights the filtering effect of the dynamics: only forcing components at or below the natural frequency are transmitted with significant amplitude, while higher harmonics are strongly attenuated. As a result, the rotor response contains far fewer spectral components than the input and their amplitudes depend on how close each harmonic lies to the resonance peak.

The envelope (third column) and its spectrum (fourth column) reveal the modulation arising from interactions between forcing harmonics and the natural mode. As shown in (22), the envelope has forcing tones, beat terms  $|1 - k\Omega_f|$ , pairwise

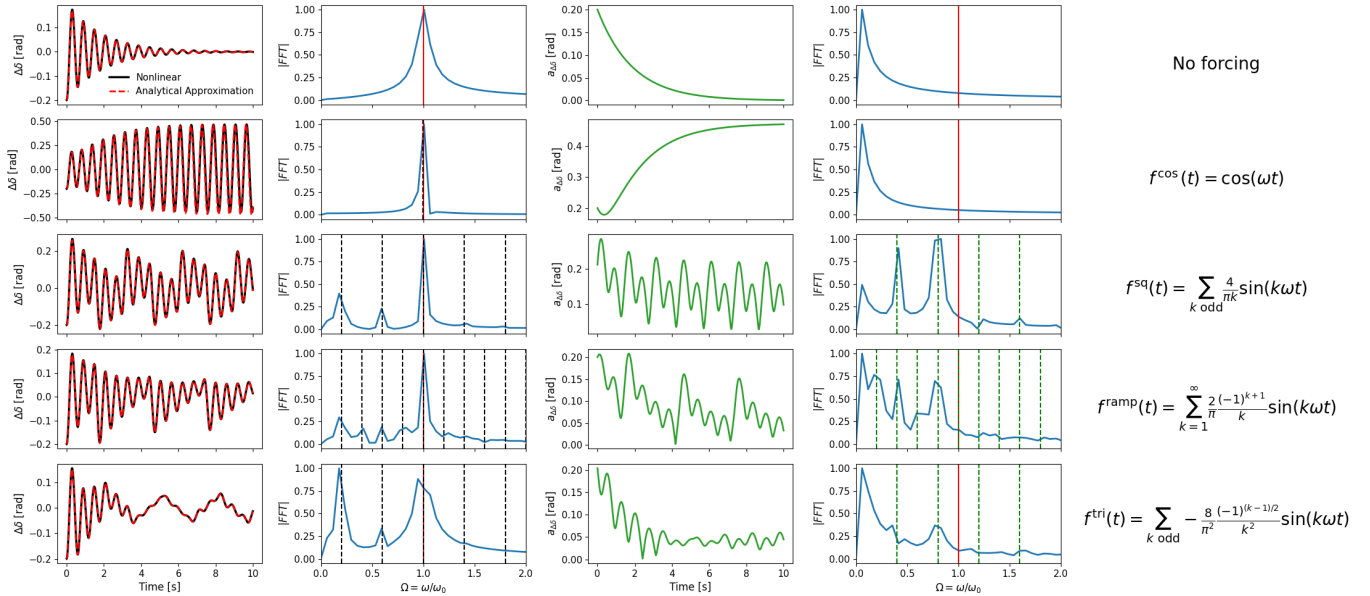


Fig. 5. Columns left to right: time-domain solution, Fourier transform, envelope, envelope spectrum and the explicit forced input.

differences  $|k - \ell|\Omega_f$  and a decaying component at  $\Omega_d$ . Ramp inputs produce a dense set of modulation frequencies because all integer harmonics are present, whereas square and triangular inputs share the same frequency structure (odd harmonics) but differ in amplitude due to their spectral decay.

The envelope FFT shows low-frequency activity associated with beat terms  $|1 - k\Omega_f|$ , which govern slow amplitude modulation and strong DC content whenever a forcing harmonic aligns with the natural frequency. The dashed green vertical lines mark the expected beat and difference frequencies listed in Table I, which match the peaks observed. Very low-frequency energy in the unforced and single-tone resonant case is produced by FFT leakage of the decaying exponential term present in (22) and does not correspond to an oscillation.

TABLE I  
ENVELOPE FREQUENCY COMPONENTS FOR DIFFERENT INPUTS.

Input	Harmonics $k$	Forcing $k\Omega_f$	Beat $ 1 - k\Omega_f $	Diff. $ k - \ell \Omega_f$
Square	1, 3, 5, 7, 9	0.2, 0.6, 1.0, 1.4, 1.8	0.8, 0.4, 0.0, 0.4, 0.8	0.4, 0.8, 1.2, 1.6
Triangular	1, 3, 5, 7, 9	0.2, 0.6, 1.0, 1.4, 1.8	0.8, 0.4, 0.0, 0.4, 0.8	0.4, 0.8, 1.2, 1.6
Ramp	1, 2, 3, 4, 5	0.2, 0.4, 0.6, 0.8, 1.0	0.8, 0.6, 0.4, 0.2, 0.0	0.2, 0.4, 0.6, 0.8

### C. Phase Plane Trajectories of Forced Oscillations

Figure 6 shows the time-evolving phase portraits of the SMIB system in coordinates  $(\Delta\delta, \Delta\omega, t)$ . Red markers are Poincaré samples taken once per forcing period, showing how the state evolves from one cycle to the next and revealing the periodic structure of the motion. Under single-tone forcing at resonance (Fig. 6a), the trajectory forms a cylindrical periodic orbit with increasing radius because the system crosses  $\Delta\delta = 0$  each cycle with progressively higher  $\Delta\omega$ .

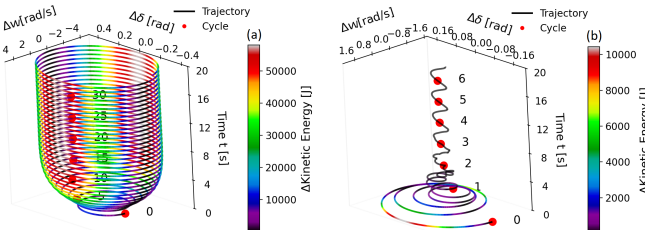


Fig. 6. Phase portraits of the SMIB system over time using equations (19) and (23). (a) Single tone cos under resonance. (b) Ramp frequency  $\omega = \omega_n/5$ .

For ramp forcing (Fig. 6b), multiple harmonics modulate the motion, producing a transient spiral in the phase plane that gradually contracts. The cycle points converge toward a fixed location, approximately  $\Delta\delta \approx 0$  and  $\Delta\omega \approx 0.065$ , indicating that forcing and damping balance at a small periodic orbit instead of amplifying toward resonance. The color scale in both cases represents kinetic energy addition to the synchronous reference, highlighting substantial energy growth at resonance and much smaller, decaying oscillations under broadband forcing.

### IV. CONCLUSION

This work developed an analytical framework to characterize multi-frequency forced oscillations in a linear SMIB subjected to mechanical forcing modeled by a finite Fourier series. Using a Laplace domain modal decomposition, the response was expressed in modal coefficients that make the harmonic participation explicit through  $\Omega = k\omega/\omega_n$ . The common denominator  $(1 - \Omega^2)^2 + (2\zeta\Omega)^2$  is the squared magnitude of a second-order transfer function, so the system behaves as a low-pass filter: for  $\Omega \ll 1$  the residues retain their full magnitude, whereas for large  $\Omega$  they decay as  $1/\Omega^2$ , strongly attenuating high frequency harmonics.

The analytic signal and the resulting envelope expression reveal how transient and steady-state components interact. The envelope contains forcing harmonics, beat terms, pairwise differences and decaying interactions with the natural mode, which in this case explains the appearance of spectral components in the envelope that were not visible in the raw time domain signal. Time-frequency maps of the envelope colored by incremental kinetic energy, together with phase plane trajectories, show that energy accumulation is tightly localized around resonance, while off-resonant components produce small, weakly modulated oscillations.

Parametric studies indicate that resonance severity is governed primarily by the magnitude and spectral content of the injected periodic mechanical disturbance and by the available damping, which shapes the height and width of the resonant peak. Inertia mainly shifts the resonance and provides a weaker amplification effect. Overall, the proposed method offers a compact and physically transparent tool to assess the dynamic behavior of multi-frequency forced oscillations and can serve as a basis for future extensions to nonlinear models and larger multi-machine power systems.

### REFERENCES

- [1] Ruichao Xie and D. Trudnowski, "Distinguishing features of natural and forced oscillations," in *2015 IEEE Power & Energy Society General Meeting*. Denver, CO, USA: IEEE, Jul. 2015, pp. 1–5.
- [2] S. A. N. Sarmadi and V. Venkatasubramanian, "Inter-Area Resonance in Power Systems From Forced Oscillations," *IEEE Trans. Power Syst.*, vol. 31, no. 1, pp. 378–386, Jan. 2016.
- [3] M. Ghorbaniparvar, "Survey on forced oscillations in power system," *J. Mod. Power Syst. Clean Energy*, vol. 5, no. 5, pp. 671–682, Sep. 2017.
- [4] L. G. Meegahapola, S. Bu, D. P. Wadduwage, C. Y. Chung, and X. Yu, "Review on Oscillatory Stability in Power Grids With Renewable Energy Sources: Monitoring, Analysis, and Control Using Synchrophasor Technology," *IEEE Trans. Ind. Electron.*, no. 1, pp. 519–531, Jan. 2021.
- [5] J. D. Follum, F. K. Tuffner, L. A. Dosiek, and J. W. Pierre, "Power System Oscillatory Behaviors: Sources, Characteristics, & Analyses," Tech. Rep. PNLL-26375, 1411936, May 2017.
- [6] H. Ye, Y. Liu, P. Zhang, and Z. Du, "Analysis and Detection of Forced Oscillation in Power System," *IEEE Trans. Power Syst.*, pp. 1–1, 2016.
- [7] Y. Zhou, J. Wu, H. Li, and Y. Li, "Analysis of Nonlinear Characteristics for Forced Oscillation Affected by Quadratic Nonlinearity," *IEEE Trans. Power Syst.*, vol. 37, no. 1, pp. 804–807, Jan. 2022.
- [8] Y. Xu, Z. Gu, K. Sun, and X. Xu, "Understanding a Type of Forced Oscillation Caused by Steam-Turbine Governors," *IEEE Trans. Energy Convers.*, vol. 35, no. 3, pp. 1719–1722, Sep. 2020.
- [9] North American Electric Reliability Corporation, "Reliability guideline: Forced oscillation monitoring & mitigation," NERC, Tech. Rep., 2017.
- [10] Lei Chen, Dan Trudnowski, Luke Dosiek, Sukumar Kamalasadan, Yanhui Xu, and Xiaozhe Wang, "Forced Oscillations in Power Systems (TR 110)," 2023, publisher: IEEE PES.